GMR
The Original

FABRICATION OF SUSTAINABLE POLYMERIC ELECTROSPUN NANOSCAFFOLDS LOADED WITH GREEN SYNTHESIZED CUO NANOPARTICLES FROM *TURBINARIA ORNATA* EXTRACT FOR ENHANCED ANTIMICROBIAL ACTIVITY

Pooja Yagavel[1], Harish Manoharan[2], David Jayaseelan Baranabas[3], Anguchamy Veeruraj[4*], Radha Mahendran[5*]

[1]Saveetha Medical College & Hospital (SMCH), Saveetha Institute of Medical and Technical Sciences (SIMATS), Thandalam, Chennai, Tamil Nadu 602105, India. poojayagavel92@gmail.com
[2]Department of Microbiology, Saveetha Medical College and Hospital, Saveetha Institute of Medical And Technical Sciences (SIMATS), Thandalam, Chennai-602105, Tamil Nadu, India. manoharan.harish@gmail.com https://orcid.org/0000-0002-8613-7440
[3]Department of Microbiology, Nehru Arts and Science College, Coimbatore-641105, Tamil Nadu, India. nascdavidjayaseelan@nehrucolleges.com; https://orcid.org/0000-0002-2619-8524
[4]Saveetha Institute of Basic Medical Sciences (SIBMS), Saveetha Medical College and Hospital, Saveetha Institute of Medical and Technical Sciences (SIMATS), Saveetha University, Chennai, 602 105, Tamil Nadu, India. anguveeruraj@gmail.com, https://orcid.org/0000-0001-7456-6507
[5]Department of Bioinformatics, School of Life Sciences, Vels Institute of Science Technology and Advanced Studies, Pallavaram, Chennai-600117, Tamil Nadu, India. Email: mahenradha@gmail.com; ORCID: https://orcid.org/0000-0003-0711-0336

ABSTRACT

TThis study investigated the green synthesis of copper oxide nanoparticles (CuO NPs) using Turbinaria ornata algal extract and their incorporation into starch/polyvinyl alcohol (PVA) electrospun nanoscaffolds for antimicrobial applications. UV-Vis spectroscopy confirmed successful biosynthesis, with the algal extract exhibiting absorption at 346 nm (indicative of phenolic/flavonoid content) and CuO NPs showing a characteristic plasmonic edge at 200 nm. Fourier Transform Infrared Spectroscopy (FTIR) analysis verified the presence of Cu-O bonds (601 cm^{-1}) in the NPs and functional groups (e.g., O-H, C=O) in the nanoscaffolds, confirming effective integration. X-ray Diffraction (XRD) confirmed the monoclinic crystalline structure of CuO NPs, while Scanning Electron Microscopy (SEM) revealed uniform, bead-free nanofibers with well-dispersed NPs. Thermogravimetric Analysis (TGA) demonstrated enhanced thermal stability in the nanocomposite, with degradation onset at 244.81°C. Dynamic Light Scattering (DLS) indicated moderate particle heterogeneity (Z-average: 92.8 nm), and zeta potential (-5.29 mV) suggested marginal colloidal stability. Antimicrobial assays against bacterial (Escherichia coli, Staphylococcus aureus) and fungal (Aspergillus niger, Penicillium spp.) pathogens revealed superior efficacy of nanoscaffolds (e.g., 29±0.19 mm for E. coli), outperforming standalone CuO NPs and algal extract. The nanoscaffolds' enhanced activity is attributed to their fibrous structure, facilitating controlled NP release. These findings highlight the potential of CuO NP-integrated nanoscaffolds as advanced antimicrobial biomaterials for wound dressings or medical coatings, while underscoring the need for stability optimization in future applications.

KEYWORDS: *Turbinaria ornata*, Green synthesis, CuO nanoparticles, Starch/PVA nanoscaffolds, Antimicrobial activity.

1. INTRODUCTION

The emergence of nanotechnology has revolutionized multiple disciplines, especially in biomedical and environmental sciences, owing to the exceptional physicochemical properties of nanomaterials such as high surface-area-to-volume ratios, unique optical behavior, and catalytic reactivity [1]. Among various metal-based nanoparticles, copper oxide nanoparticles (CuO NPs) have garnered substantial interest due to their cost-effectiveness, eco-friendliness, redox activity, and broad-spectrum antimicrobial potential [2]. These properties make CuO NPs attractive for a wide array of applications, including biosensing, catalysis, drug delivery, and wound healing [3]. Despite the versatility of CuO NPs, their synthesis method plays a crucial role in defining their morphology, size distribution, surface properties, and, consequently, their biological interactions and functional efficacy [4].

Traditional chemical and physical methods for synthesizing metal oxide nanoparticles are often energy-intensive, expensive, and reliant on toxic chemicals that pose environmental and health hazards [5]. To mitigate these drawbacks, green synthesis techniques have emerged as sustainable and eco-conscious alternatives [6]. These approaches harness natural reducing agents present in plant extracts, fungi, bacteria, or algae to facilitate nanoparticle formation under mild conditions [7]. Among these biological agents, marine macroalgae (seaweeds) represent a promising and underexplored source of phytochemicals that serve dual functions as reducing and stabilizing agents during nanoparticle synthesis [8]. Marine macroalgae are rich in diverse bioactive compounds, including polysaccharides, phenolics, alkaloids, terpenoids, and flavonoids, all of which contribute to metal ion reduction and nanoparticle stabilization [9].

Turbinaria ornata, a brown macroalga widely distributed in tropical and subtropical coastal waters, is particularly noteworthy due to its rich phytochemical composition [10]. Traditionally, T. ornata has been utilized in folk medicine for its therapeutic attributes, including antibacterial, antifungal, antioxidant, and anti-inflammatory properties [11]. Recent studies have reported the potential of this seaweed as a biogenic source for nanoparticle synthesis [12]. The polyphenolic content, coupled with sulfated polysaccharides in T. ornata, provides a conducive medium for the green synthesis of metal oxide nanoparticles with desirable physicochemical and biological properties [13]. However, limited literature exists on the integration of T. ornata-mediated CuO NPs into functional polymeric platforms, particularly for biomedical applications such as antimicrobial wound dressings [14].

The current study capitalizes on the green synthesis potential of T. ornata for fabricating CuO NPs, which are subsequently incorporated into a nanofibrous scaffold matrix composed of starch and polyvinyl alcohol (PVA) [15]. Electrospinning, a versatile and scalable technique for fabricating nanofibers, was employed to produce CuO-loaded starch/PVA scaffolds [16]. Electrospun nanofibers are well-suited for biomedical applications owing to their high porosity, surface-area-to-volume ratio, and the ability to mimic the extracellular matrix (ECM), thus promoting cellular adhesion, proliferation, and differentiation [17]. PVA, a biocompatible and biodegradable synthetic polymer, is often employed in electrospinning due to its favorable spinnability, mechanical strength, and aqueous solubility [18]. However, PVA lacks inherent biological activity and is typically blended with natural polymers such as starch to enhance its biofunctionality [18].

Starch, a naturally abundant and renewable polysaccharide, exhibits excellent biocompatibility, film-forming ability, and hydrophilicity, making it an ideal additive for biomedical scaffolds [19]. When blended with PVA, starch improves the scaffold's biodegradability and water uptake capacity while maintaining mechanical integrity [18]. Additionally, the incorporation of bioactive nanoparticles such as CuO further enhances the antimicrobial and antioxidant properties of the scaffold, making it suitable for applications such as wound healing, infection control, and tissue engineering [20].

The green-synthesized CuO NPs in this study were characterized using various analytical techniques including UV–Visible spectroscopy, Fourier Transform Infrared Spectroscopy (FTIR), X-ray Diffraction (XRD), Scanning Electron Microscopy (SEM), Thermogravimetric Analysis (TGA), Dynamic Light Scattering (DLS), and zeta potential measurements [21]. These characterization tools provided a comprehensive understanding of the nanoparticles' structural, morphological, thermal, and colloidal properties [22]. The optical properties were assessed via UV–Vis spectroscopy to confirm the formation of CuO NPs and identify characteristic surface plasmon resonance (SPR) peaks [23]. FTIR analysis elucidated the functional groups involved in nanoparticle stabilization, while XRD provided insights into the crystalline structure and phase purity of the synthesized nanoparticles [24]. SEM imaging revealed the morphology and distribution of nanoparticles within the electrospun fibers, and TGA established the thermal stability and degradation profile of the composite scaffolds [25]. DLS and zeta potential analysis helped determine the particle size distribution and surface charge, which are critical parameters influencing colloidal stability and biological interactions [26].

In addition to physicochemical characterization, the antimicrobial efficacy of the biosynthesized CuO NPs and CuO-loaded nanofibrous scaffolds was rigorously assessed against clinically relevant bacterial and fungal pathogens, including Escherichia coli, Klebsiella pneumoniae, Staphylococcus aureus, Citrobacter koseri, Aspergillus niger, and Penicillium spp. [27]. Using the agar well diffusion assay, this study compared the antimicrobial activity of the T. ornata extract, synthesized CuO NPs, and the composite nanofibrous scaffolds [28]. The zone of inhibition measurements served as a direct indicator of the bacteriostatic or fungistatic potential of the developed materials, with larger inhibition zones denoting superior antimicrobial performance [29]. The findings underscore the potential of the CuO NP-loaded starch/PVA nanofibers as effective antimicrobial materials with significant relevance in wound care and infection prevention [30].

The integration of green nanotechnology with electrospinning opens new avenues for developing multifunctional, biocompatible scaffolds tailored for biomedical use [31]. In particular, marine-derived biomolecules offer a sustainable and potent platform for nanoparticle synthesis, aligning with global efforts toward eco-conscious manufacturing practices [32]. By harnessing the reducing and capping capabilities of T. ornata, this study not only mitigates the environmental footprint associated with conventional nanoparticle synthesis but also adds value to marine biodiversity [33].

This work presents a comprehensive approach to developing antimicrobial electrospun scaffolds by leveraging the green synthesis of CuO NPs using T. ornata extract and embedding them into starch/PVA nanofibers [34]. The successful fabrication and characterization of the CuO NP-loaded scaffolds and their demonstrated antimicrobial activity support their potential use in biomedical applications, particularly in wound management [35]. The outcomes of this study contribute valuable insights into the synergistic integration of marine phytochemicals, nanotechnology, and polymer science to produce next-generation biomaterials for healthcare solutions [36].

2. MATERIALS AND METHODS

2.1. Materials

This study utilized T. ornata macroalgae, sourced from Rameswaram, Tamil Nadu, India, for the green fabrication of CuO NPs. Copper(II) sulfate pentahydrate ($CuSO_4 \cdot 5H_2O$), obtained from Sigma-Aldrich, served as the metal salt precursor. PVA (MW ~115,000) was selected as the base polymer for electrospinning, while starch from a local supplier was blended to improve scaffold functionality. All solvents and reagents, including ethanol and Milli-Q water, were of analytical grade and purchased from Merck and Sigma-Aldrich. The electrospinning was conducted using a HOLMARC HO-NFES-040 unit equipped with a syringe pump. Characterization tools included UV-Vis spectroscopy (VIS SPEC V-730), FTIR (Spectrum Two, PerkinElmer), XRD (Bruker D8 Advance), SEM (JSM-IT800 NANO), and particle analysis using zeta potential and DLS (Malvern Zetasizer Ultra), as well as thermal profiling with TGA 8000 (PerkinElmer).

2.2. Marine macroalgae collection

T. ornata specimens were harvested from the seashores near Rameswaram, Tamil Nadu, India. The collected *Turbinaria Ornata* was taxonomically identified and authenticated by Dr V. Veeragurunathan, CSIR-CSMCRI-Marine Algal Research Station, Mandapam Camp 623519, Tamil Nadu, India. A voucher specimen was prepared and deposited at the Herbarium of the CSIR-CSMCRI-Marine Algal Research Station, under the accession number: SI–2025–RMM–022. This authentication ensures botanical accuracy and standardization of the study material. The freshly collected samples were thoroughly cleaned using tap water to eliminate surface debris, followed by rinsing with distilled water to ensure the removal of residual contaminants. Approximately 100 grams of the cleaned algae were then chopped into small sections and air-dried under ambient conditions for about two weeks. Once dried completely, the biomass was ground into a fine powder using a mechanical grinder, which was then stored and used for further experimental steps.

2.3. Ultrasonic-assisted extraction

To isolate bioactive constituents, 2 g of the powdered T. ornata were suspended in 50 mL of Milli-Q water in a 100 mL glass beaker. The suspension was subjected to ultrasonic-assisted extraction using a LABQUEST ultrasonic cleaner (Borosil; Serial No. 941032329018) at 60°C for a duration of 45 minutes. Following sonication, the mixture was filtered using Whatman No. 1 filter paper under sterile conditions. The clear filtrate obtained was transferred to a sterile 50 mL container and stored at 10°C. For future applications, the liquid extract was converted into powder form through lyophilization using a freeze dryer [37, 38].

2.4. Green synthesis of CuO NPs

Green synthesis of CuO NPs was achieved by mixing 50 mL of 0.1 M $CuSO_4 \cdot 5H_2O$ with 10 mL of aqueous T. ornata extract (prepared by dissolving 10 mg in 10 mL Milli-Q water) at a volumetric ratio of 5:1. This solution was continuously stirred at 650 rpm and maintained at 60°C for 2 hours on a magnetic hot plate. The appearance of a bluish-green hue from the initial blue indicated nanoparticle formation. The synthesized particles were washed three times with double-distilled water using identical stirring and heating conditions. The final product was freeze-dried over a period of 48 hours and stored as a powdered form for further analysis [39].

2.5. Fabrication of electrospun starch/PVA scaffolds containing CuO NPs

A 15% (w/w) solution of fully hydrolyzed PVA in water was prepared for scaffold fabrication. Into this, 100 mg each of starch and biosynthesized CuO NPs were added and stirred intensively at 50°C for 2.5 hours for uniform dispersion. The prepared solution was loaded into a syringe fitted with a 0.84 mm diameter needle and electrospun using a HOLMARC HO-NFES-040 setup, powered by a HMPSKV30 supply (0–30 kV, 0.5 mA). Optimized electrospinning settings included a voltage of 11.5 kV, needle-to-collector gap of 12.3 cm, and flow rate of 0.4 mL/h. The electrospinning was carried out at room temperature for 6–8 hours to produce fibrous mats [40-42].

2.6. Physicochemical characterization

2.6.1. UV–visible spectroscopy analysis

To verify optical characteristics and initial nanoparticle formation, UV–Visible spectroscopy was used. Spectral scans were performed on three separate samples: T. ornata extract, green-synthesized CuO NPs, and CuO-loaded starch/PVA electrospun scaffolds. Measurements were taken using a VIS SPEC V-730 UV–Vis spectrophotometer across a wavelength range of 200 to 800 nm to detect electronic transitions. Deionized water was used as a blank to calibrate the instrument for baseline correction. This facilitated the identification of surface plasmon resonance (SPR) peaks and interactions within the polymer-nanoparticle system [43].

2.6.2. FTIR spectroscopy analysis

Fourier Transform Infrared Spectroscopy was used to identify functional groups and bonding features in the materials. A Spectrum Two FTIR spectrometer (PerkinElmer) operating in ATR mode was employed. Spectra for T. ornata extract, CuO NPs, and CuO-integrated starch/PVA nanofibers were recorded within 4000–400 cm^{-1}, using a fixed resolution of 4 cm^{-1}. Each spectrum was averaged over 64 scans to improve signal clarity. The analysis identified key chemical groups such as -OH, C=O, amide, and M-O bonds, offering molecular-level insights into structural components and interactions within the composites [44].

2.6.3. XRD analysis

The crystalline nature and phase integrity of the CuO NPs and nanoparticle-loaded electrospun mats were analyzed using X-ray diffraction. A Bruker D8 Advance diffractometer with CuKα radiation (λ = 1.5406 Å) was used under conditions of 40 kV and 40 mA. Scans were performed from 5° to 90° (2θ) with a step size of 0.029649°. Diffraction patterns were examined for peaks associated with monoclinic CuO, and any shifts or broadening were noted to determine nanoparticle incorporation into the polymer scaffold [45].

2.6.4. SEM analysis

Morphological features of CuO NPs and their distribution within the starch/PVA matrix were observed using a JEOL JSM-IT800 NANO SEM. Prior to imaging, samples were sputter-coated with gold to enhance conductivity and avoid charging under the electron beam. SEM micrographs provided high-resolution visualization of particle morphology, dispersion quality, potential clustering of CuO NPs, and fiber structure and alignment within the scaffold [46].

2.6.5. TGA evaluation

Thermal stability and degradation characteristics of the CuO NP-loaded scaffolds were examined using TGA via a PerkinElmer TGA 8000 instrument. Around 5 mg of each sample was placed in aluminum crucibles and subjected to

heating from room temperature to 550°C at a rate of 15°C/min in a nitrogen environment to avoid oxidation. The resulting thermograms helped determine water loss, thermal stability, and degradation stages of the polymer composite [47].

2.6.6. Zeta potential and particle size distribution

To evaluate colloidal behavior, the hydrodynamic size and zeta potential of the green-synthesized CuO NPs were analyzed using a Malvern Zetasizer Ultra. DLS assessed particle size, while zeta potential measured surface charge. These analyses revealed nanoparticle dispersion and stability; higher absolute zeta potential values indicated improved colloidal stability in aqueous environments. Combined data provided a comprehensive physicochemical profile [48].

All characterization data have been deposited and made publicly available via Mendeley Data (DOI: 10.17632/tgxw2g4stx.1) to support data transparency and reproducibility.

2.7. Evaluation of antimicrobial properties

The agar well diffusion method was employed to examine the antimicrobial effects of T. ornata extract (50 µg/mL), CuO NPs (50 µg/mL), and starch/PVA electrospun nanoscaffolds (50 µg/mL) on selected bacterial and fungal strains, including Escherichia coli, Klebsiella pneumoniae, Staphylococcus aureus, Citrobacter koseri, Aspergillus niger, and Penicillium species.

Microbial suspensions were adjusted to a 0.5 McFarland standard for uniformity and spread onto Mueller-Hinton agar (for bacteria) and Sabouraud dextrose agar (for fungi). Wells (6 mm in diameter) were created in the agar, and 50 µL of each test sample (50 µg/mL) along with positive controls (ciprofloxacin for bacteria and voriconazole for fungi) were dispensed into the wells.

After a 30-minute pre-diffusion period, the plates were incubated at 37°C for 24 hours (bacteria) or 28°C for 48 hours (fungi). Following incubation, the antimicrobial efficacy was quantified by measuring the diameter (in millimeters) of the inhibition zones surrounding the wells, where larger zones correlated with greater antimicrobial potency. To ensure reproducibility, the experiment was performed in triplicate [49, 50].

2.8. Data analysis

Statistical evaluation was carried out using SPSS version 25.0 and GraphPad Prism 9.0 software. Results, presented as mean ± standard deviation (SD) from triplicates, were analyzed using one-way ANOVA for variance between groups. Post hoc tests such as Tukey's or Dunnett's were applied for multiple comparisons, and significance was accepted at $p < 0.05$. Pearson's correlation assessed relationships between variables, while normality was confirmed via Shapiro-Wilk test. Where data deviated from normality, logarithmic transformation was applied. A 95% confidence level was maintained for all inferential analyses [51].

3. RESULTS

3.1. UV–visible spectroscopy

The UV-Vis spectra (Figure 1) of the T. ornata algal extract and biosynthesized CuO NPs revealed distinct optical signatures. The algal extract exhibited a broad absorption band spanning 200–400 nm, with maximum absorbance (1.943) at ~346 nm, characteristic of conjugated systems in phenolic compounds, flavonoids, and chlorophyll derivatives. In contrast, the CuO NPs displayed a sharp absorption edge at ~200 nm, indicative of surface plasmon resonance (SPR) associated with their nanoscale dimensions and electronic transitions. The absence of overlapping peaks between the extract (organic phytochemicals) and NPs (inorganic phase) confirmed successful biosynthesis. These results validate the extract's role as a reducing/capping agent in CuO NP synthesis and demonstrate effective NPs incorporation into the nanofibrous matrix, with optical properties suitable for applications requiring UV absorption or photocatalytic activity.

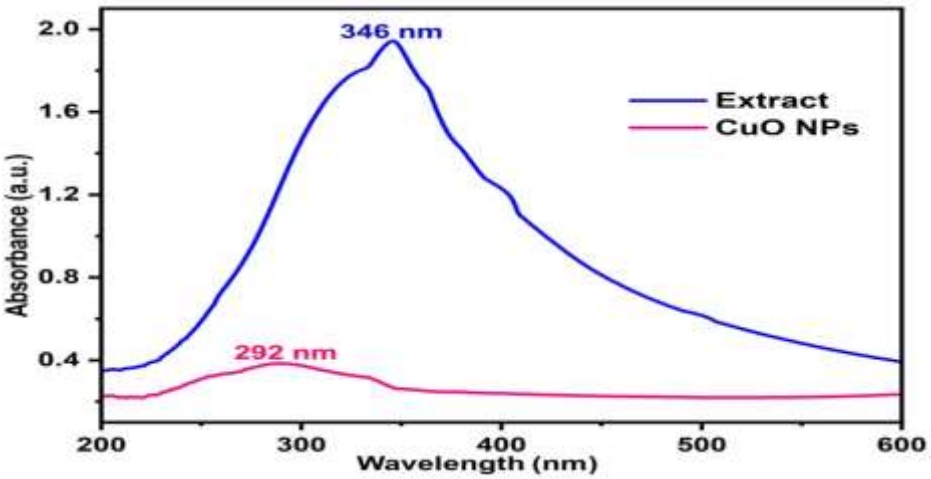

Figure 1. UV–Visible spectral profiles of algal extract and CuO NPs.

3.2. FTIR spectroscopy analysis

FTIR analysis (Figure 2) of the CuO NPs and nanoscaffolds revealed distinct functional group signatures. The CuO NPs spectrum exhibited characteristic peaks at 601 cm^{-1} (Cu-O stretching vibrations), 863 cm^{-1} (metal-oxygen bonds), and 1061 cm^{-1} (C-O stretching), along with a broad band at 3122 cm^{-1} (O-H stretching from surface-adsorbed water or algal phytochemicals). In contrast, the nanoscaffolds displayed prominent peaks at 3284 cm^{-1} (O-H/N-H stretching from

PVA/starch), 2921 cm^{-1} (C-H stretching), 1710 cm^{-1} (C=O carbonyl groups), and 1424 cm^{-1} (C-H bending), confirming the polymeric matrix composition. Notably, the presence of peaks at 1328 cm^{-1} (C-N/O-H bending) and 1087 cm^{-1} (C-O-C glycosidic linkages) in the nanoscaffolds, along with residual Cu-O vibrations (604 cm^{-1}), verified successful CuO NP incorporation into the fibrous network. The absence of peak overlap between the CuO NPs and scaffold materials demonstrated phase purity, while the persistence of algal-derived functional groups on CuO NPs highlighted their bio-capped nature. These results collectively confirm the chemical integrity of both components and their effective integration in the composite scaffold

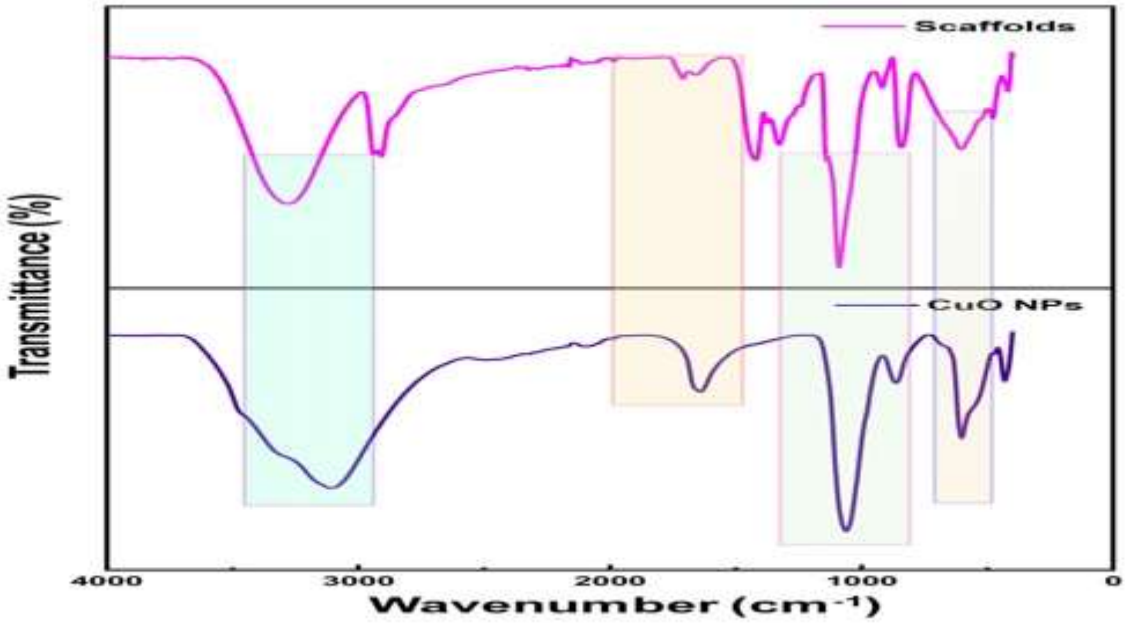

Figure 2. FTIR spectra of CuO NPs and their incorporation into nanoscaffolds.

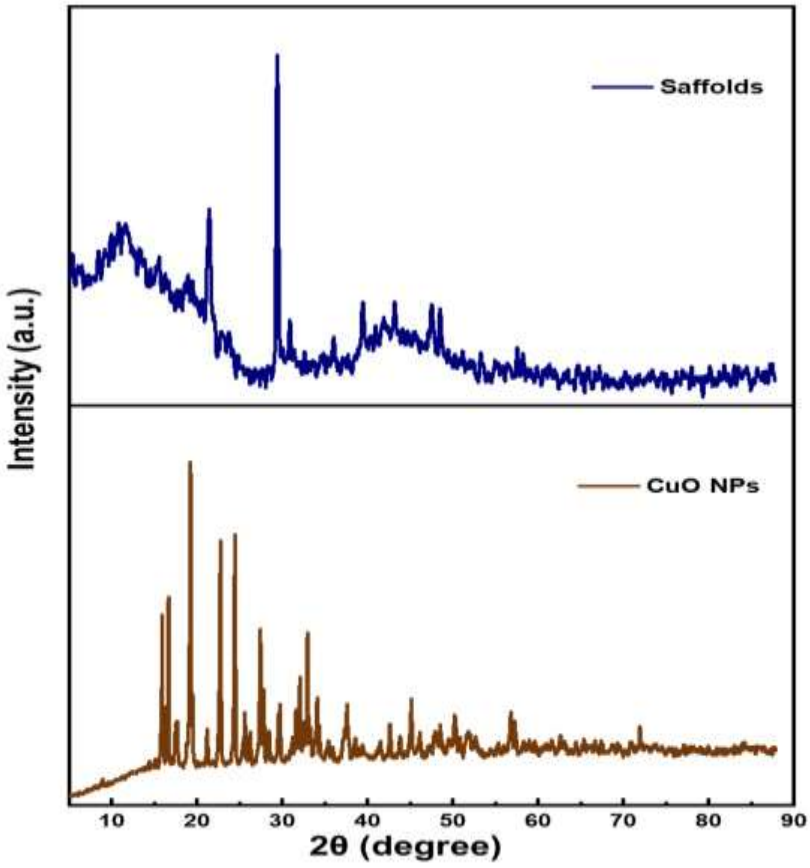

Figure 3. XRD patterns of synthesized CuO NPs and CuO-loaded scaffolds.

3.3. XRD analysis

XRD analysis (Figure 3) was performed to investigate the crystallographic structure and phase purity of the biosynthesized CuO NPs and the electrospun nanoscaffolds incorporating these NPs. The study utilized a Bruker D8 Advance diffractometer with CuKα radiation (λ = 1.5406 Å) under operating conditions of 40 kV and 40 mA. The samples were

scanned over a 2θ range of 5° to 90° with a step size of 0.029649°. For the CuO NPs, the XRD pattern revealed 28 distinct diffraction peaks at 15.862°, 16.582°, 17.564°, and up to 71.876°, corresponding to d-spacings ranging from 5.58251 Å to 1.31247 Å. The most intense peak at 24.435° (d = 3.64001 Å, 100% relative intensity) confirmed the monoclinic phase of CuO (JCPDS card no. 48-1548), while other peaks such as 32.876° (d = 2.72213 Å) and 38.504° (d = 2.33623 Å) further validated the crystalline structure. The nanoscaffolds exhibited fewer peaks, with notable ones at 21.420° (d = 4.14507 Å), 29.372° (d = 3.03842 Å, 100% relative intensity), and 57.572° (d = 1.59965 Å), indicating a combination of crystalline and amorphous phases (17.4% crystallinity). Peak broadening in the nanoscaffolds, evidenced by higher FWHM values (e.g., 0.525° at 30.771°), suggested reduced crystallinity due to the polymeric matrix. The absence of impurity peaks confirmed the phase purity of CuO NPs, while shifts in peak positions and intensities in the nanoscaffolds highlighted successful nanoparticle incorporation and their influence on the scaffold's structural properties. This analysis conclusively demonstrated the monoclinic crystalline nature of CuO NPs and their integration into the nanoscaffolds, with minimal phase alteration.

3.4. SEM analysis

SEM analysis (Figure 4) of the green-synthesized CuO NPs and CuO NPs-integrated starch/PVA electrospun nanoscaffolds revealed distinct morphological characteristics under high-resolution imaging. The CuO NPs exhibited a predominantly spherical to slightly irregular shape with a size range of 70–90 nm, though some agglomeration was observed due to their high surface energy. In contrast, the electrospun starch/PVA nanoscaffolds displayed uniform, bead-free fibers with smooth surfaces and an average diameter of 150–300 nm, confirming successful fiber formation. The incorporation of CuO NPs into the nanofibrous matrix was evident, with nanoparticles evenly distributed along the fiber surfaces and minimal large-scale aggregation, suggesting effective dispersion during electrospinning. However, localized clusters of CuO NPs were occasionally detected, likely due to interfacial interactions between the NPs and polymer matrix. The nanofibers demonstrated good continuity and alignment, with a porous network structure conducive to potential biomedical applications. These findings confirm the successful synthesis of CuO NPs and their integration into the nanoscaffolds while highlighting the need for optimized dispersion techniques to further reduce NPs agglomeration. The SEM results collectively provide critical insights into the structural integrity and nanoscale organization of both the standalone CuO NPs and their composite scaffolds

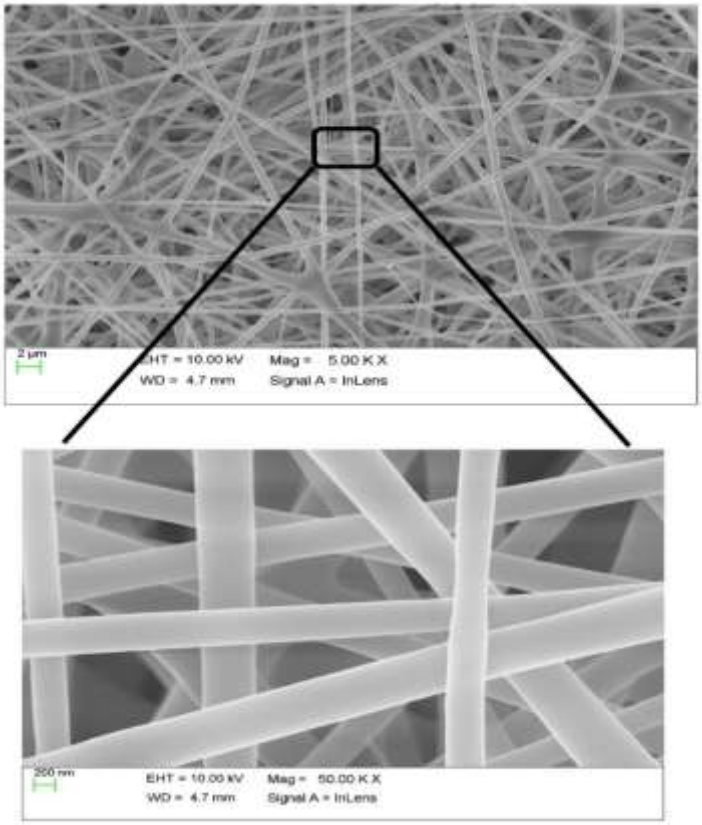

Figure4. SEM analysis of starch/PVA/CuO-NPs nanoscaffolds

3.5. TGA evaluation

The thermal stability and decomposition behavior of the CuO NPs-integrated starch/PVA nanofibrous scaffolds were evaluated using thermogravimetric analysis (Figure 5) performed on a PerkinElmer system. A sample weighing 2.315 mg was heated from 30.00°C to 550.00°C at a rate of 15.00°C/min under a nitrogen atmosphere. The thermogram revealed a multi-stage degradation process, with an initial weight loss of 9.509% attributed to moisture evaporation and volatile content. The primary decomposition stage exhibited an onset temperature of 244.81°C, a peak degradation temperature at 332.83°C, and an endpoint at 378.85°C, corresponding to the thermal breakdown of the starch/PVA polymeric matrix. The derivative weight curve (%/min) highlighted the maximum degradation rate at 332.83°C, while the total weight loss reached 41.696% by 550°C, indicating significant polymer decomposition. The presence of CuO NPs likely influenced

the thermal stability, as evidenced by the residual mass and shifted degradation profile compared to pure polymer scaffolds. These results confirm the composite's thermal behavior, with the nanoparticles potentially enhancing the scaffold's thermal resistance by delaying polymer chain scission

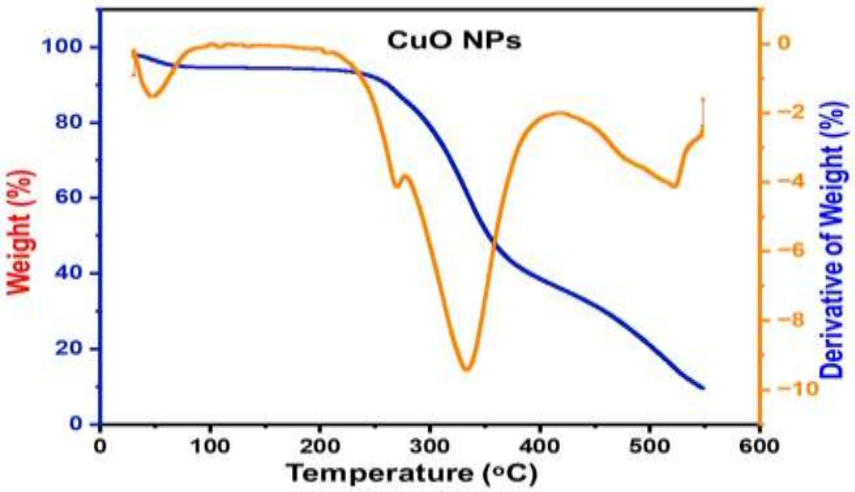

Figure 5. Thermal degradation behavior of CuO-incorporated nanoscaffolds.

3.6. Zeta potential and particle size analysis

The colloidal stability and hydrodynamic size of the biosynthesized CuO NPs were analyzed using a Malvern Panalytical Zetasizer. DLS revealed a bimodal particle size distribution with yielding a Z-average size of 92.8 nm (Figure 6) and a polydispersity index (PI) of 0.5592, indicating moderate size heterogeneity. The derived mean count rate was 3465 kcps, reflecting stable dispersion dynamics. Zeta potential analysis demonstrated a mean surface charge of -5.29 mV, with a conductivity of 0.1086 mS/cm and a zeta deviation of 6.424 mV (Figure 7), suggesting weak electrostatic repulsion and marginal colloidal stability in aqueous media. The low absolute zeta potential value ($< \pm 10$ mV) implies a tendency toward aggregation, corroborated by the broad size distribution. These results highlight the need for surface modification to enhance stability for biological or environmental applications, as the current formulation may exhibit limited long-term dispersion integrity.

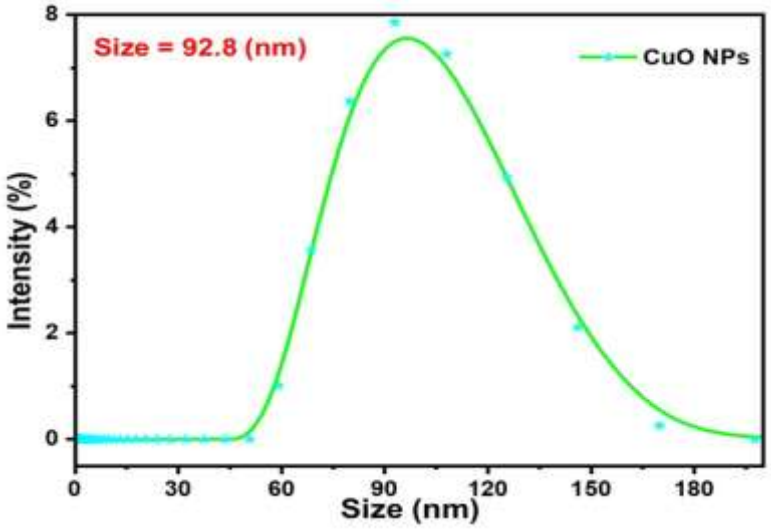

Figure6. DLS particles size analysis of CuO NPs

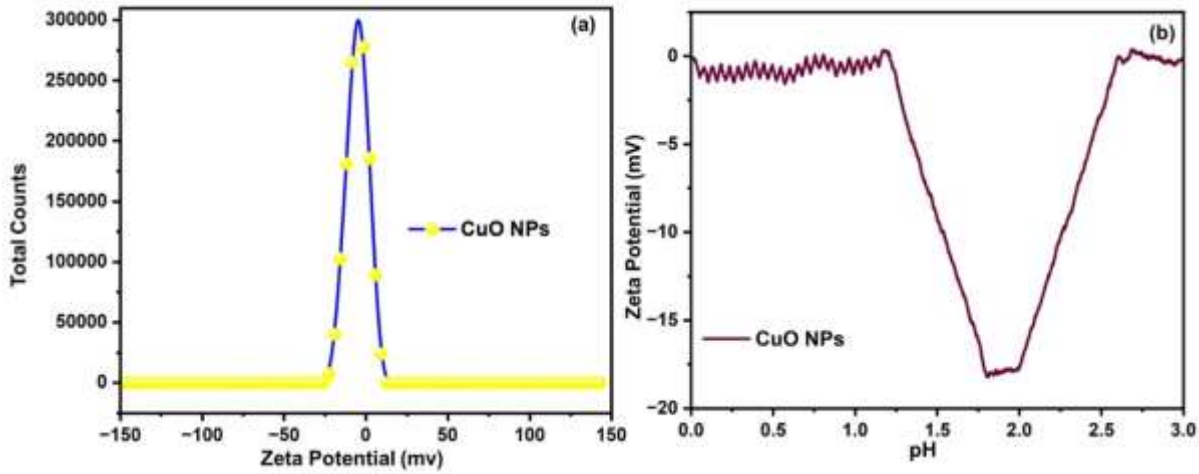

Figure7. Zeta-potential analysis of CuO NPs

3.7. Antimicrobial properties evaluation

The agar well diffusion method was utilized to assess the antimicrobial activity of T. ornata extract (50 µg/mL), CuO NPs (50 µg/mL), and starch/PVA electrospun nanoscaffolds (50 µg/mL) against pathogenic bacteria (Escherichia coli, Klebsiella pneumoniae, Staphylococcus aureus, Citrobacter koseri) and fungi (Aspergillus niger, Penicillium species). Microbial suspensions were standardized to a 0.5 McFarland standard and inoculated onto Mueller-Hinton agar (bacteria) or Sabouraud dextrose agar (fungi). Wells (6 mm diameter) were filled with 50 µL of each test sample or controls (ciprofloxacin for bacteria, voriconazole for fungi). After a 30-minute pre-diffusion period, plates were incubated at 37°C (24 hours for bacteria) or 28°C (48 hours for fungi). The results demonstrated varying inhibition zones: for E. coli, the algal extract showed moderate activity (15±0.18 mm), while CuO NPs exhibited lower efficacy (20±0.22 mm), and nanoscaffolds displayed strong inhibition (29±0.19 mm), comparable to ciprofloxacin (33±0.58 mm). Similar trends were observed for K. pneumoniae (14±0.27 mm, 19±0.13 mm, 27±0.23 mm) and S. aureus (13±0.23 mm, 17±0.24 mm, 24±0.15 mm). Against fungi, the algal extract (12±0.14 mm for A. niger, 13±0.22 mm for Penicillium) and CuO NPs (15±0.14 mm, 17±0.22 mm) showed modest activity, whereas nanoscaffolds achieved significant inhibition (22±0.16 mm, 24±0.27 mm), though less than voriconazole (26±0.65 mm, 28±0.39 mm). Triplicate experiments confirmed reproducibility, highlighting the nanoscaffolds' superior antimicrobial potential compared to the extract and CuO NPs.

Table 1: Antimicrobial activity of T. ornata extract, CuO NPs, and starch/PVA electrospun nanoscaffolds at concentration of 50 µg/mL against various pathogenic organisms.

Organisms	Zone of inhibition (mm)				
	Ciprofloxacin (Antibiotic)	Voriconazole (Antifungal)	Algal Extract	CuO NPs	Nano-scaffolds
Escherichia coli	33±0.58	-	15±0.18	20±0.22	29±0.19
Klebsiella pneumoniae	30±0.14	-	14±0.27	19±0.13	27±0.23
Staphylococcus aureus	28±0.32	-	13±0.23	17±0.24	24±0.15
Citrobacter koseri	29±0.47	-	14±0.12	18±0.21	25±0.28
Aspergillus niger	-	26±0.65	12±0.14	15±0.14	22±0.16
Penicillium species	-	28±0.39	13±0.22	17±0.22	24±0.27

4. DISCUSSION

The green synthesis and characterization of CuO NPs using T. ornata extract, followed by their integration into electrospun starch/PVA nanoscaffolds, demonstrated promising physicochemical and biological properties suitable for biomedical applications. The findings from various characterization techniques substantiate the successful synthesis, integration, and potential utility of the fabricated nanoscaffolds [52].

The UV–Visible spectroscopic analysis revealed distinct optical features for both the algal extract and the biosynthesized CuO NPs. The algal extract exhibited a broad absorption band in the UV region (200–400 nm), with a strong absorption peak centered at 346 nm. This peak is indicative of the presence of conjugated π-electron systems, typically associated with phenolic compounds, flavonoids, and chlorophyll derivatives—phytochemicals known to act as natural reducing and capping agents during nanoparticle biosynthesis. In contrast, the CuO NPs demonstrated a sharp absorption edge around 200 nm, characteristic of surface plasmon resonance (SPR) related to electronic transitions in nanoscale metal oxides. The lack of spectral overlap between the extract and nanoparticle absorption bands suggests successful synthesis and phase separation. This observation reinforces the role of T. ornata extract in mediating the reduction and stabilization of CuO NPs while confirming the optical purity and potential for photocatalytic or UV-protective applications [53-56].

FTIR spectra provided detailed insights into the functional groups present in both the CuO NPs and nanoscaffold composites. The CuO NPs exhibited signature peaks corresponding to Cu–O stretching vibrations around 601 and 863 cm^{-1}, confirming the formation of the metal oxide. Additional peaks observed at 1061 and 3122 cm^{-1} were attributed to C–O stretching and surface O–H stretching, respectively, likely arising from bioorganic compounds in the algal extract adhered to the nanoparticle surface. The presence of such phytochemical residues further supports the green synthesis pathway. The nanoscaffolds, on the other hand, exhibited prominent polymeric peaks, including O–H/N–H stretching (3284 cm^{-1}), C–H stretching (2921 cm^{-1}), carbonyl C=O groups (1710 cm^{-1}), and bending vibrations (1424 cm^{-1}), all of which confirmed the integrity of the starch/PVA matrix. The observed peaks for C–N and glycosidic linkages, along with persistent Cu–O vibrations, confirm not only the incorporation of CuO NPs into the scaffolds but also their stable interaction with the polymer matrix [24, 57].

The crystallographic analysis using XRD provided further confirmation of the phase purity and structural characteristics of the biosynthesized CuO NPs and their incorporation into the nanoscaffolds. The CuO NPs exhibited sharp, intense peaks corresponding to the monoclinic phase of CuO (JCPDS card no. 48-1548), affirming their high crystallinity and successful formation. Notable diffraction peaks at 24.435°, 32.876°, and 38.504° corresponded to well-defined crystal planes, confirming the material's nanoscale crystalline structure. Upon incorporation into the polymeric nanoscaffolds, the intensity and number of diffraction peaks diminished, accompanied by peak broadening. This can be attributed to the amorphous nature of the PVA/starch matrix and partial disruption of long-range order due to nanoparticle dispersion within the polymer. The estimated crystallinity of 17.4% and absence of secondary phases or impurity peaks further confirmed the homogeneous dispersion of CuO NPs without structural compromise [58, 59].

SEM imaging revealed detailed morphological features of both the nanoparticles and nanoscaffolds. The CuO NPs presented as predominantly spherical structures ranging from 70–90 nm in diameter, with some tendency toward agglomeration due to high surface energy and lack of strong electrostatic repulsion. In contrast, the electrospun nanoscaffolds showed uniform, bead-free fiber formation with smooth surfaces, averaging 150–300 nm in diameter. The incorporation of CuO NPs into the fibrous matrix was clearly evident, with even distribution and minimal aggregation. Occasional localized clusters indicated partial nanoparticle–polymer interfacial interactions. Importantly, the fibrous network exhibited high porosity and alignment, characteristics advantageous for tissue engineering and drug delivery applications where gas exchange and nutrient diffusion are critical [60].

TGA provided insights into the thermal degradation behavior of the nanocomposite scaffolds. A multi-step decomposition pattern was observed, with an initial mass loss attributed to moisture evaporation followed by a major degradation phase commencing around 244°C and peaking at 332.83°C. This corresponds to the breakdown of the starch and PVA components. The final weight loss (~41.7%) by 550°C, along with residual mass, suggests that CuO NPs contributed to improved thermal resistance by possibly inhibiting polymer chain mobility and delaying scission. Such thermal stability is crucial for sterilization and storage of biomaterials [61-63].

DLS and zeta potential analyses were performed to evaluate colloidal properties. The CuO NPs displayed a Z-average size of 92.8 nm suggests some degree of nanoparticle clustering. A low zeta potential value of -5.29 mV suggests insufficient electrostatic repulsion, corroborating SEM observations of mild agglomeration. This indicates a need for further stabilization strategies, such as surface functionalization, for long-term aqueous suspension stability [64-67].

The study evaluated the antimicrobial efficacy of T. ornata extract, CuO NPs, and starch/PVA electrospun nanoscaffolds against bacterial and fungal pathogens using the agar well diffusion method. The results revealed distinct antimicrobial profiles for each test material. The algal extract exhibited moderate activity, with inhibition zones ranging from 12±0.14 mm (Aspergillus niger) to 15±0.18 mm (Escherichia coli), suggesting its potential as a natural antimicrobial agent. However, its performance was inferior to conventional antibiotics like ciprofloxacin (33±0.58 mm for E. coli). CuO NPs demonstrated limited efficacy, with zones between 15±0.14 mm (A. niger) and 20±0.22 mm (E. coli), likely due to their lower bioavailability or slower release kinetics [68-71].

In contrast, the starch/PVA nanoscaffolds displayed the strongest antimicrobial effects, with inhibition zones nearing those of standard antibiotics (e.g., 29±0.19 mm for E. coli). This superior performance may stem from their electrospun structure, which enhances surface area and active compound release. The nanoscaffolds also showed notable antifungal activity (22±0.16 mm for A. niger), though slightly less than voriconazole (26±0.65 mm).

These findings highlight the promise of nanoscaffolds as advanced antimicrobial materials, combining biocompatibility (starch/PVA) with potent efficacy. Future research should optimize their formulation for clinical applications, such as wound dressings or coatings for medical devices. Meanwhile, the algal extract and CuO NPs, while less effective, could serve as complementary agents in combination therapies or low-resource settings. The study underscores the importance of innovative biomaterials in addressing antibiotic resistance.

5. CONCLUSION

This study successfully demonstrated the green synthesis of CuO NPs using *T. ornata* extract and their effective incorporation into electrospun starch/PVA nanofibrous scaffolds. Spectroscopic analyses confirmed the distinct optical and structural features of both the bioactive extract and the synthesized nanoparticles, validating the role of phytochemicals in nanoparticle formation and stabilization. FTIR and XRD analyses substantiated the chemical integrity, phase purity, and crystalline structure of the CuO NPs and their seamless integration within the polymeric matrix. SEM images revealed uniform fiber morphology with well-dispersed nanoparticles, while TGA indicated enhanced thermal stability due to the presence of CuO NPs. Zeta potential analysis reflected moderate colloidal stability, suggesting potential improvements via surface modification. Importantly, antimicrobial assessments revealed that the nanoscaffolds exhibited significantly higher inhibitory activity against bacterial and fungal pathogens compared to the extract or nanoparticles

alone. Overall, the synthesized CuO NP-integrated nanoscaffolds exhibit promising potential for future biomedical applications, especially in antimicrobial wound dressing development.

Ethical Declaration: Not applicable for this study.

Funding: Not available for this study.

Conflicts of Interest: The authors declare no conflicts of interest.

Data Availability Statement: The full dataset of physiochemical characterization associated with this work is published in Mendeley Data [Dataset] Eco-friendly nanocomposite scaffolds: physicochemical analysis of starch matrices integrated with *Turbinaria ornata*-mediated CuO nanoparticles (DOI: 10.17632/tgxw2g4stx.1). Disclosure: The material characterization data and figures (e.g., UV, SEM, FTIR, XRD, TGA, Zeta Potential and particle sizer) presented here were generated from a common dataset and are being reused across multiple related studies on nanomaterials. All biological analyses and conclusions are original to each manuscript.

REFERENCES

1. Singh N, Kumar B, Usman UL, Susan MABH. Nano revolution: exploring the frontiers of nanomaterials in science, technology, and society. Nano-Structures & Nano-Objects. 2024;39:101299.
2. Jiang H, Kumarasamy RV, Pei J, Raju K, Kanniappan GV, Palanisamy CP. Integrating engineered nanomaterials with extracellular vesicles: Advancing targeted drug delivery and biomedical applications. Frontiers in Nanotechnology. 2024; 6: 1513683.
3. Guo H, Liu Y, Wan T, Song D, Palanisamy CP, Geng J, Pei J, Özmen S, El-Aty AMA. Toward personalized cancer management: Role of precision nutrition–diet interventions. Journal of Functional Foods. 2024; 123: 106584.
4. Natarajan SR, Krishnamoorthy R, Alshuniaber MA, Al-Anazi KM, Farah MA, Rajagopal P, Palanisamy CP, Veeraraghavan VP, Jayaraman S. Identification of FOXM1 as a novel protein biomarker and therapeutic target for colorectal cancer progression: Evidence from immune infiltration and bioinformatic analyses. International Journal of Biological Macromolecules. 282 (Part 4): 137201.
5. Rajendran MS, Jayaraman S, Khan JM, Jasmine S, Prabhakaran RK, Raju MV, Chandrasekaran MK, Ahalliya RM, Kannappan P, Palanisamy CP, Kanniappan GV. Investigating the colon toxicity and carcinogenic role of monosodium glutamate compared with Dimethylhydrazine in male Wistar rats: Exploring the link to childhood colon cancer risk. Journal of King Saud University - Science. 2024; 36(11): 103507.
6. Kumarasamy RV, Natarajan PM, Umapathy VR, Roy JR, Rab SO, Saeed M, Panagal M, Mironescu M, Srinivasan GP, Palanisamy CP. Clinical Applications and Therapeutic Potentials of Advanced Nanoparticles: A Comprehensive Review on Completed Human Clinical Trials. Frontiers in Nanotechnology. 2024; 6:1479993.
7. Jin W, Pei JJ, Roy JR, Jayaraman S, Ahalliya RM, Kanniappan GV, Mironescu M, Palanisamy CP. Comprehensive review on single-cell RNA sequencing: A new frontier in Alzheimer's disease research. Ageing Research Reviews. 2024; 274: 102454.
8. Pei J, Palanisamy CP, Jayaraman S, Natarajan PM, Umapathy VR, Roy JR, Panagal M, Jayaraman S. Curcumin-loaded polymeric nanomaterials as a novel therapeutic strategy for Alzheimer's disease: A comprehensive review. Ageing Research Reviews. 2024; 99: 102393.
9. Pei J, Palanisamy CP, Jayaraman S, Natarajan PM, Umapathy VR, Roy JR, Thalamati D, Ahalliya RM, Kanniappan GV*, Mironescu M. A comprehensive review on starch-based Sustainable Edible Films Loaded with Bioactive Components for Food Packaging. International Journal of Biological macromolecules. 2024; 274 (Part-1): 133332.
10. Palanisamy CP, poompradub S, Sansanaphongpricha K, Subramani K, Sonsudin F. Increased expression levels of PDGF and VEGF magnify the wound healing potential facilitated by biogenic synthesis of silver nanoparticles. Nano-Structures & Nano-Objects. 2024; 39: 101236.
11. Pei J, Palanisamy CP, Jayaraman S, Natarajan PM, Umapathy VR, Roy JR, Thalamati D, Ahalliya RM, Kanniappan GV, Mironescu M. Proteomics Profiling of Extracellular Vesicle for Identification of Potential Biomarkers in Alzheimer's Disease: A Comprehensive Review. Ageing Research Reviews. 2024; 99: 102359.
12. Xi J, Wang T, Xian P, Liu X, Du M, Yang H, Palanisamy CP, Lin W, Long Q. Proteomic insights uncover enhanced neurotherapeutic potential in conditioned mesenchymal stem cell-derived extracellular vesicles. Extracellular Vesicle. 2024; 3: 100037.
13. Pei J, Natarajan PM, Umapathy VR, Swamikannu B, Sivaraman NM, Krishnasamy L, Palanisamy CP. Advancements in the synthesis and functionalization of zinc oxide-based nanomaterials for enhanced oral cancer therapy. Molecules. 2024; 29(11): 2706.
14. Gatasheh MK, Natarajan SR, Krishnamoorthy R, Alsulami TS, Rajagopal P, Palanisamy CP, Veeraraghavan VP, Jayaraman S. Molecular analysis to identify novel potential biomarkers as drug targets in colorectal cancer therapy: an integrated bioinformatics analysis. Molecular and Cellular Oncology. 2024; 11(1): 2326699.
15. Pei J, Yan Y, Jayaraman S, Rajagopal P, Natarajan PM, Umapathy VR, Gopathy S, Roy JR, Sadagopan CS, Thalamati D, Palanisamy CP, Mironescu M. A review on advancements in the application of starch-based nanomaterials in biomedicine: Precision drug delivery and cancer therapy. International Journal of Biological Macromolecules. 2024; 130746.

16. Pei JJ, Yan Y, Palanisamy CP, Jayaraman S, Natarajan PM, Umapathy VR, Gopathy S, Roy JR, Sadagopan JC, Thalamati D, Mironescu M. Materials-based drug delivery approaches: Recent advances and future perspectives. Green Processing and Synthesis. 2024; 13: 20230094.
17. Panneerselvam S, Viswaja K, Deepa E, Prathiba S, Rebecca FS, Nivedha RP, Rajagopal P, Veeraraghavan VP, Sridevi G, Palanisamy CP, Jayaraman S. Hypoglycemic Potential of Acalypha indica in Streptozotocin-Induced Type 2 Diabetic Rats. International Journal of Drug Delivery Technology. 2026; 16(26s):1038-1047.
18. Panneerselvam S, Viswaja K, Prathiba S, Rebecca FS, Nivedha RP, Rajagopal P, Fathima SJH, Veeraraghavan VP, Sridevi G, Palanisamy CP, Jayaraman S. Acalypha Indica Attenuates Insulin Resistance in STZ-Induced Type 2 Diabetic Male Rats: Mechanistic Study. International Journal of Drug Delivery Technology. 2026; 16(26s):1027-1037.
19. Manju NE, Natarajan A, Rebecca FS, Nivedha RP, Hemalatha R, Rajagopal P, Murali R, Veeraraghavan VP, Sridevi G, Palanisamy CP, Jayaraman S. Effect of Seendhil polyherbal formulation in attenuating type-2 diabetes in STZ-induced experimental rats. International Journal of Drug Delivery Technology. 2026; 16(26s):981-989.
20. Manju NE, Natarajan A, Rebecca FS, Nivedha RP, Hemalatha R, Rajagopal P, Murali R, Veeraraghavan VP, Sridevi G, Palanisamy CP, Jayaraman S. Molecular mechanism to identify the effects of Seendhil polyherbal preparation on IRS-1/AKT/GLUT4/NRF2-KEAP-1 mediated signaling in SFZ-induced type-2 diabetic adult male rats. International Journal of Drug Delivery Technology. 2026;16(26s):972-980.
21. Palanisamy CP, Poompradub S, Sansanaphongpricha K, Jayaraman S, Subramani K, Sonsudin F. Biosynthesis of silver nanoparticles (AgNPs) using ethanolic extract of Nigella sativa (L.) seeds promotes wound healing via PDGF and VEGF signalling pathways activation. Biocatalysis and Agricultural Biotechnology. 2023; 54: 102970.
22. Palanisamy CP, Pei JJ, Phaniendra A, Venkata AAN, Jayaraman S, Veeraragahavan VP, Sridevi G, Roy JR, Janaki CS, Thalamati D, Mironescu M, Luo Q, Chai Y, Long Q. New Strategy of Neurodegenerative Disease Treatment with Extracellular Vesicles (EVs) Derived from Mesenchymal Stem Cells (MSCs). Theranostics. 2023; 13(12):4138-4165.
23. Natarajan PM. Dental Bioinformnatics-Current Scope and Future perspectives. Research Journal of Pharmacy and Technology. 2022;15(5):2351-6.
24. Vidhyarekha U, Natarajan PM, Bhuminathan S, Sabarinathan J, Suba R, Vijayalakshmi P. Role of artificial intelligence in Oral Cancer. Advances in Public Health. 2024. 2024: 3664408.
25. Ganesan A, Kumar NG, Natarajan PM, Gauthaman J. Automated classification of elongated styloid processes using deep learning models-an artificial intelligence diagnostics. Frontiers in Oral Health. 2025; 5: 1424840.
26. Umapathy VR, Natarajan PM, Swamikannu B. Regenerative Strategies in Dentistry: Harnessing Stem Cells, Biomaterials and Bioactive Materials for Tissue Repair. Biomolecules. 2025; 15: 546.
27. Natarajan PM, Umapathy VR, Murali A, Swamikannu B. (2022). Computational Simulations of Identified marine-derived Natural Bioactive Compounds As Potential Inhibitors of Oral Cancer. Future Science OA. 2022; 8(3).
28. Ganesan A, Kumar NG, Natarajan PM. Solanum trilobatum leaf extract-derived silver nanoparticles downregulate the PI3K/AKT/mTOR signaling pathway and attenuate oral squamous cell carcinoma cell proliferation. Journal of Herbmed Pharmacology. 2024; 13(2): 300-307.
29. Perumal MKK, Renuka RR, Subbiah SK, Natarajan PM. Artificial intelligence-driven clinical decision support systems for early detection and precision therapy in oral cancer: a mini review. Frontiers in Oral Health. 2025; 6: 1592428.
30. Ramesh E, Ganesan A, Lakshmi KC, Natarajan PM. Artificial intelligence-based diagnosis of oral leukoplakia using deep convolutional neural networks Xception and MobileNet-v2. Frontiers in Oral Health. 2025; 6: 1414524.
31. Natarajan PM. Computational Studies on Recent Congeners of Fluoroquinolones and Nitroimidazoles for Their Use in Periodontal Therapy. Journal of Pharmacy and Bioallied Sciences. 2024; 16(5): S4731-S4740.
32. Ganesan A, Kumar NG, Natarajan PM. Anticancer activity of silver nanoparticles synthesized from aqueous leaf extract of Solanum trilobatum (Purple fruit pea eggplant) on human oral cancer cells. Journal of Herbmed Pharmacololgy. 2024; 13(2): 260-268.
33. Umapathy V, Dhanavel A, Kesavan R, Natarajan PM, Bhuminathan S, Vijayalakshmi P. Anticancer Potential of the Principal Constituent of Piper nigrum, Piperine: A Comprehensive Review. Cureus. 2024; 16(2): e54425.
34. Natarajan PM, Bhuminathan S, Rajan R, Bindu K, Loganathan K, Veerakumar R. The Crucial Role of Smoking Cessation in Preventing Oral Cancer. Journal of Pharmacy and Bioallied Sciences. 2024; 16(5): S4245-S4247.
35. Umapathy VR, Swamikannu B, Natarajan PM, Devi R, Nandini MS, Vimalarani, Vijayalakshmi P. In Silico Molecular Docking of Ocimum sanctum Phytochemicals: Targeting Key Biomarkers in Oral Cancer. Journal of Pharmacy and Bioallied Sciences. 2024; 16(5): S4792-S4799.
36. Natarajan PM, Umapathy VR. Role of transcriptomics in the study of oral cancer. Frontiers in Oral Health. 2025; 6:1524364.
37. Swamikannu B, Umapathy VR, Natarajan PM, Nandini MS, Stylin AGSQ, Vimalarani V, Rajinikanth S. Unlocking the Therapeutic Benefits of Artemisia Annua: A Comprehensive Overview of its Medicinal Properties. Journal of Pharmacy and Bioallied Sciences. 2024; 16(5): S4248-S4253.
38. Yadalam PK, Arumuganainar D, Natarajan PM, Ardila CM. Artificial intelligence-powered prediction of AIM-2 inflammasome sequences using transformers and graph attention networks in periodontal inflammation. Scientific Reports. 2025; 15: 8733.
39. Yadalam PK, Chatterjee S, Natarajan PM, Ardila CM. Comparison of light gradient boosting and logistic regression for interactomic hub genes in Porphyromonas gingivalis and Fusobacterium nucleatum-induced periodontitis with Alzheimer's disease. Frontiers in Oral Health. 2025; 6:1463458.
40. Natarajan PM, Bhuminathan S, Leela B, Bindu K, Loganathan K, Ramachandran V. Smoking and its Role in Oral Cancer. Journal of Pharmacy and Bioallied Sciences 16(5): S4242-S4244.

41. Yadalam PK, Natarajan PM, Ardila CM. Variational graph autoencoder for reconstructed transcriptomic data associated with NLRP3 mediated pyroptosis in periodontitis. Scientific Reports. 2025; 15: 1962.
42. Natarajan PM, Swamikannu B, Sivaraman NM, Stylin AGSQ. Prevention of Oral Cancer: A Comprehensive Guide. Journal of Pharmacy and Bioallied Sciences. 2024; 16(5): S4239-S4241.
43. Surendran N, Chandrasekaran G, Raju MV, Chandrasekaran MK, Ahalliya RM, Palanisamy CP, Kanniappan GV, Arcot R, Alharbi NS, Thiruvengadam M. Anti-inflammatory potential of ethanolic extract of Maranta arundinacea L.: Insights from COX-2 modulation and oxidative stress analysis. South African Journal of Botany. 2026; 195: 142-151.
44. Pei J, Senthilkumar MV, Hessini K, Subramaniyam S, Sivaramakrishnan R, Kanniappan GV, Jayaraman S, Palanisamy CP. Green fabrication of starch/PVA/CuO nanoscaffolds using marine macroalgae extract for enhanced anti-inflammatory activity. Sustainable Chemistry and Pharmacy. 2026; 51: 102397.
45. Balasubramanian V, Loganathan L, Muthuswamy K, Viswanathan TM, Raju MV, Chandrasekaran MK, Ahalliya RM, Poorasamy J, Palanisamy CP, Dominic S, Kanniappan GV. Anticancer therapeutic efficacy of PEGylated β-galactosidase from Aspergillus terreus in DMBA-induced breast cancer: Toxicological, molecular and histopathological evaluation in Wistar rats. International Journal of Biological Macromolecules. 2026; 360: 151856.
46. Jayaraman S, Eswaran A, Rajagopal P, Palanisamy CP, Veerakumar P, Veeraraghavan VP, Sirasanagandla SR. Neuroendocrine-associated epigenetic factors in cellular senescence: mechanisms and therapeutic implications. Biogerontology. 2026; 27(2): 64.
47. Ponnusamy B, Rajagopal P, Palanisamy CP, Veeraraghavan VP, Jayaraman S. Mechanistic Exploration of the anticancer activity of Justicia adhatoda Plant Leaf Ethanolic Extract against Colon Cancer Cells: An in silico and in vitro Approach. Asian Pacific Journal of Cancer Prevention. 2026; 27(3): 1069-1080.
48. Pei J, Saran VS, Sivaramakrishnan R, Kanniappan GV, Pandurangan V, Jayaraman S, Dhayalan VK, Mironescu M, Mironescu ID, Palanisamy CP. Ultrasonic-assisted, Sargassum ilicifolium (brown marine macroalgae)-mediated biogenic synthesis of CuO nanoparticles incorporated in starch/PVA electrospun nanoscaffolds: In vitro safety and antioxidant efficacy assessment. Bioorganic Chemistry. 2026; 173: 109679.
49. Raj MAPA, Subramaniyam S, Kanniappan GV, Jayaraman S, Palanisamy CP. Sustainable fabrication of starch/PVA/CuO electrospun nanoscaffolds from Turbinaria ornata (marine macroalgae) extract: Physicochemical characterization and antidiabetic evaluation. Kuwait Journal of Science. 2026; 53(2): 100545.
50. Pei J, Ganesh NS, Subramaniyam S, Sivaramakrishnan R, Kanniappan GV, Jayaraman S, Palanisamy CP. Sustainable fabrication of starch/PVA/CuO electrospun nanoscaffolds from Padina tetrastromatica (Brown macroalgae) extract: Physicochemical characterization and antidiabetic assessment. Sustainable Chemistry One World. 2026; 9: 100195.
51. Sakthiraj A, Sivaramakrishnan R, Subramaniyam S, Kanniappan GV, Pandurangan V, Jayaraman S, Dhayalan VK, Mironescu M, Mironescu ID, Palanisamy CP. Chemical Physics Impact. Starch/PVA electrospun nanoscaffolds loaded with ultrasonic-assisted green-synthesis of CuO nanoparticles from marine macroalgae (Gracilaria corticata) extract: Cytotoxicity and antioxidant analysis. 2026; 12: 101018.
52. Raju M, Chandrasekaran MK, Loganathan L, Ahalliya RM, Mironescu M, Mironescu ID, Palanisamy CP, Kanniappan GV. Lipid remodeling and ferroptosis in phosphatidylcholine-mediated tumor–stroma crosstalk. Frontiers in Molecular Biosciences. 2026; 13: 1742305.
53. Kunamalla R, Panagal M, Palanisamy CP. Biogenic synthesis and fabrication of starch/PVA/CuO electrospun nanoscaffolds from Sargassum ilicifolium (brown marine macroalgae) extract for anticancer activity on HT-29 and MCF-7 cancer cells. Biocatalysis and Agricultural Biotechnology. 2026; 72: 103923.
54. Pei J, Govindaraj H, Sivaramakrishnan R, Kanniappan GV, Pandurangan V, Dhayalan VK, Mironescu M, Mironescu ID, Jayaraman S, Palanisamy PC. Sustainable fabrication of biopolymer-based (starch/PVA) nanoscaffolds loaded with green-synthesized CuO nanoparticles from Sargassum wightii (marine macroalgae): Cytocompatibility and antioxidant activity. Biomaterials Advances. 2026; 182: 214660.
55. Pei J, Perumal NC, Meng P, Long Q, Palanisamy CP. Extracellular vesicle-based biosensors for Alzheimer's disease: A new frontier in precision diagnostics. Ageing Research Reviews. 2026; 113: 102904.
56. Shree P, Sivaramakrishnan R, Kanniappan GV, Pandurangan V, Jayaraman S, Dhayalan VK, Mironescu M, Mironescu ID, Palanisamy CP. Antioxidant and biocompatible CuO-starch/PVA nanoscaffolds via ultrasonic green synthesis using Turbinaria conoides (brown marine macroalgae). Medicine in Drug Discovery. 2025; 28: 100238.
57. Gong J, Lin J, Guan T, Pei J, Palanisamy CP, El-AtyFrom AMA. selenium tolerance to nanoplastic antagonism: Comprehensive characterization of L. casei SNUT1 and its extracellular vesicle–nanoselenium complex. Food Bioscience. 2025; 74: 107749.
58. Poochi SP, Sundarraj R, Raju MV, Chandrasekaran MK, Ahalliya RM, Palanisamy CP, Kanniappan GV, Kondapavuluri BK, Thiruvengadam M. Harnessing Nature: Computational and Experimental Insights Into Ipomoea obscura Metabolites for Bladder Cancer Therapy. Chemistry and Biodiversity. 2025; 0: e00909.
59. Dugganaboyana GK, Kannankumar MKG, Shivaramakrishna S, Raju MV, Chandrasekaran MK, Ahalliya RM, Panneerselvam N, Palanisamy CP, Kanniappan GV. Phytochemical insights, antioxidant activity and therapeutic potential of Cassia senna against prostate cancer in Wistar albino rats. Discover Applied Sciences. 2025; 7:1206.
60. Natarajan SR, Krishnamoorthy R, Alshuniaber MA, Gatasheh MK, Rajagopal P, Veeraraghavan VP, Palanisamy CP, Jayaraman S. KDM1A Facilitates Oncogenic Potential in Colorectal Cancer Progression Through the Activation of AXIN/GSK3β/β-Catenin Signaling Pathways: Evidence From Integrated Transcriptomics and In Vitro Studies. The Journal of Gene Medicine. 2025; 27(11): e70053.
61. Guan T, Gong J, Lin J, Palanisamy CP, Jinjin Pei J, El-Aty AMA. Machine learning-driven multimodal optimization of selenium biotransformation and flavor profiling in fermented apple–Yacon functional beverages. Innovative Food Science & Emerging Technologies. 2025; 105: 104198.

62. Natarajan SR, Krishnamoorthy R, Alshuniaber MA, Alsulami TS, Gatasheh MK, Rajagopal P, Palanisamy CP, Govindan R, Veeraraghavan VP, Jayaraman S. ABCE1 facilitates tumour progression via aerobic glycolysis and inhibits cell death in human colorectal cancer cells through the p53 signalling pathway. Scientific Reports. 2025; 15: 24674.
63. Huang Y, Guo H, Liu Y, Jin W, Palanisamy CP, Pei J, Oz F, El-Aty AMA. Effects of Natural Polysaccharides on the Gut Microbiota Related to Human Metabolic Health. Molecular Nutrition & Food Research. 2025; 69:e202400792.
64. Poornima K, Meenakshi K.C, Manikandan V.R, Shankari G, Prabhu D, Rathi M.A, Palanisamy CP, Balaji R, Gopalakrishnan V.K. Exploring the anticancer potential of Jerantinine A from Tabernaemontana coronaria against prostate, breast, and ovarian cancers: A computational approach. Journal of Complementary and Integrative Medicine, 2025 22(2): 363–372.
65. Palanisamy CP, Poompradub S, Sansanaphongpricha K, Jayaraman S, Subramani K. Faridah Sonsudin gGreen synthesis of Nigella sativa-mediated silver nanoparticles for enhanced antibacterial activity and wound healing: Mechanistic insights and biomedical applications. Environmental Nanotechnology, Monitoring & Management. 2025; 24: 101085.
66. Surendran N, Raju MV, Chandrasekaran MK, Ahalliya RM, Palanisamy CP, Chandrasekaran G, Kanniappan GV. Physicochemical characterization of starch from Maranta arundinacea L.(arrowroot) rhizomes and its inhibition of COX-2: In vivo validation. Bioactive Carbohydrates and Dietary Fibre. 2025; 33: 100465.
67. Kannappan P, Chandrasekaran MK, Raju MV, Gopalakrishnan S, Dhamodharan P, Ahalliya RM, Palanisamy CP, Raju B, Kanniappan GV. Exploring the anticancer potential of Jerantinine A from Tabernaemontana coronaria against prostate, breast, and ovarian cancers: a computational approach. Journal of Complementary and Integrative Medicine. 2025; 22(02): 363-372.
68. Pei J, Kumarasamy RV, Jayaraman S, Kanniappan GV, Long Q, Palanisamy CP. Quercetin-functionalized nanomaterials: Innovative therapeutic avenues for Alzheimer's disease management. Ageing Research Reviews. 2025; 104: 102665.
69. Jayaraman S, Prasad M, Natarajan SR, Krishnamoorthy R, Alshuniaber MA, Gatasheh MK, Veeraraghavan VP, Rajagopal P, Palanisamy CP. Molecular mechanisms underlying the effects of beta-sitosterol on TGF-β1/Nrf2/SIRT1/p53-mediated signaling in the kidney of a high-fat diet and sucrose-induced type-2 diabetic rat. Chemico-Biological Interactions. 2025; 411: 111443.
70. Huang Y, Guo H, Liu Y, Jin W, Palanisamy CP, Pei J, Oz F, El-Aty AMA. Effects of Natural Polysaccharides on the Gut Microbiota Related to Human Metabolic Health. Molecular Nutrition & Food Research. 2025; e202400792.
71. Prabhakaran P, Palanisamy CP, Shanmugam A, Damodharan P, Swaminathan H, Devaraj D, Ahalliya RM, Kanniappan GV. Isolation, structural characterization, and molecular docking studies on the bioactive compound from n-Hexane extract of Emilia sonchifolia (L.) DC against the pancreatic cancer target Aurora 2 Kinase. Journal of Complementary and Integrative Medicine. 2024; 22(1): 0290.